

Majorana Zero Mode Detected with Spin Selective Andreev Reflection in the Vortex of a Topological Superconductor

Hao-Hua Sun,¹ Kai-Wen Zhang,² Lun-Hui Hu,^{3,4} Chuang Li,^{3,4} Guan-Yong Wang,¹ Hai-Yang Ma,¹ Zhu-An Xu,^{3,4} Chun-Lei Gao,^{1,4} Dan-Dan Guan,^{1,4} Yao-Yi Li,^{1,4} Canhua Liu,^{1,4} Dong Qian,^{1,4} Yi Zhou,^{3,4} Liang Fu,⁵ Shao-Chun Li,^{2,4,*} Fu-Chun Zhang,^{3,4,†} and Jin-Feng Jia^{1,4,‡}

¹Key Laboratory of Artificial Structures and Quantum Control (Ministry of Education), Department of Physics and Astronomy, Shanghai Jiao Tong University, Shanghai 200240, China

²National Laboratory of Solid State Microstructures and School of Physics, Nanjing University, Nanjing 210093, China

³Department of Physics, Zhejiang University, Hangzhou 310027, Zhejiang, China

⁴Collaborative Innovation Center of Advanced Microstructures, Nanjing 210093, China

⁵Department of Physics, Massachusetts Institute of Technology, Cambridge, Massachusetts 02139-4307, USA

(Received 5 April 2016; revised manuscript received 16 May 2016; published 21 June 2016)

Recently, theory has predicted a Majorana zero mode (MZM) to induce spin selective Andreev reflection (SSAR), a novel magnetic property which can be used to detect the MZM. Here, spin-polarized scanning tunneling microscopy or spectroscopy has been applied to probe SSAR of MZMs in a topological superconductor of the $\text{Bi}_2\text{Te}_3/\text{NbSe}_2$ heterostructure. The zero-bias peak of the tunneling differential conductance at the vortex center is observed substantially higher when the tip polarization and the external magnetic field are parallel rather than antiparallel to each other. This spin dependent tunneling effect provides direct evidence of MZM and reveals its magnetic property in addition to the zero energy modes. Our work will stimulate MZM research on these novel physical properties and, hence, is a step towards experimental study of their statistics and application in quantum computing.

DOI: 10.1103/PhysRevLett.116.257003

The Majorana fermion (MF) is a special type of fermion whose antiparticle is itself [1]. The MF was initially proposed in elementary particle physics, and the recent effort in searching such a genuine particle focuses on the neutrinoless double beta decay experiment [2]. The Majorana zero mode (MZM), which follows the Majorana equation that describes MFs, may emerge as a novel excitation in some condensed matter systems. MZMs obey non-Abelian statistics and may be used as robust building blocks in quantum computing [3,4]. Chiral p -wave superconductors [5] and the $\nu = 5/2$ fractional quantum Hall system [6] are possible candidates to host MZM [6]. Fu and Kane proposed the existence of MZMs at the interface of a topological insulator (TI) and an s -wave superconductor (SC) [7]. In recent years, a number of proposals have been explored to detect the MZM, including the experiments in one-dimensional (1D) Rashba semiconducting wire [8–11] and 1D Fe atom chains on Pb [12]. Topological superconductivity may be induced on surfaces of 3D TIs such as Bi_2Se_3 , Bi_2Te_3 , and Sb_2Te_3 via the proximity effect, and the localized MZM at the vortex core has been studied by using scanning tunneling microscopy or spectroscopy (STM/STS) [13–15]. However, there are quasiparticle states inside the vortex core, whose lowest energies cannot be distinguished from the zero modes within the present STM energy resolution. This introduces great difficulty in detection of the MZM by using normal STM/STS with a nonpolarized tip. He *et al.* have recently proposed a novel

property of MZM in a 1D system [16], where the Andreev reflection (AR) is spin selective. They showed that MZM induces selective equal spin AR, in which incoming electrons with certain spin polarization in the lead are reflected as counterpropagating holes with the same spin [7]. The proposed spin selective AR (SSAR) of the MZM in 1D wire can be generalized to a 2D topological superconductor (TSC). In the latter case, the spin of the MZM in the vortex core has a spatial distribution and is not conserved [15]. However, we note that the spin wave function at the center of the vortex core $r = 0$ of the Majorana mode is fully polarized along the external magnetic field, with r the lateral distance of the tip from the vortex center; see Fig. 3(a). Therefore, the AR at $r = 0$ is expected to be spin selective, and can be probed in spin polarized (SP) STM/STS [16–18].

A unique advantage to probe SSAR in the TSC is that a small magnetic field is sufficient to induce vortices and, hence, the spin-polarized MZM in the vortex core. On the other hand, the spin polarization of surface states and finite-energy quasiparticle states is still negligibly small, as we can see in Fig. 3(b) below. In other systems, it is required to apply a sufficiently large magnetic field to make the system topological in the first place, in which case the bands are already spin polarized. It will then be difficult to attribute spin-dependent zero-bias conductance to the MZM since both MZM (if present) and finite-energy midgap states would be spin polarized.

Tip polarization parallel with the M field Tip polarization antiparallel with the M field

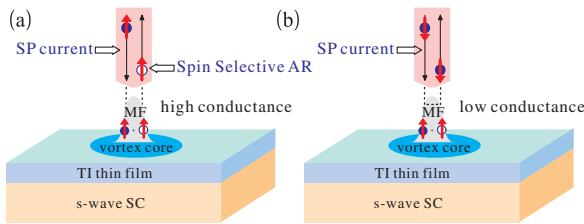


FIG. 1. (a) Illustration of spin selective Andreev reflection in spin polarized ($M\uparrow$) STM/STS on a vortex center $r = 0$ in an interface of a topological insulator and s -wave superconductor. An incoming spin-up electron of zero energy is reflected as an outgoing spin-up hole induced by Majorana zero mode with spin-up at $r = 0$, which gives out a higher tunneling conductance. (b) An incoming spin-down electron of zero energy is reflected directly because of the mismatch of the spins of the electron and the Majorana zero mode, which results in a lower tunneling conductance.

In Fig. 1, we illustrate SSAR induced by the MZM at the vortex center of an interface of TI and SC. The tunneling conductance consists of two parts,

$$\frac{dI(r, E; \hat{B}, \hat{M})}{dV} = \left. \frac{dI(r, E; \hat{B}, \hat{M})}{dV} \right|_n + \left. \frac{dI(r, E; \hat{B}, \hat{M})}{dV} \right|_A, \quad (1)$$

where the first term is the contribution from the normal tunneling, and the second term from the AR. E is the energy, \hat{B} and \hat{M} are the orientations of the external magnetic field B and spin polarization M , respectively. Note that the spin selective AR is most profound at $r = 0$, where the superconducting order parameter vanishes; hence, the AR is purely induced via the MZM. Hereafter, we shall focus on the discussion for low energy spectra at $r = 0$ unless explicitly specified otherwise. $dI/dV|_n$ is proportional to the local density of states, which is independent of spin polarization at $r = 0$ and $E = 0$ within the energy resolution of about 0.1 meV (see model calculation part below). Therefore, we expect that the first term in Eq. (1) is independent of spin polarization, and the difference of spin-dependent conductance probes the SSAR.

In this work, we report the observation of the MZM via SP-STM/STS measurements. Ferromagnetic Fe/W tips are applied to probe vortex core states in a 5 quintuple layers (QL) $\text{Bi}_2\text{Te}_3/\text{NbSe}_2$ heterostructure, where the topological superconductivity has been established [13]. The intensity of the zero bias peak (ZBP) at the vortex center is observed to be dependent on the magnetic polarization M of the applied tip, and it is 14% higher for M parallel rather than antiparallel to the applied magnetic field B . We attribute the spin-dependent tunneling to the SSAR, a special novel property of the MZM in TSC. The experimental observation is in good agreement with a model calculation.

The experiments were performed in an ultrahigh vacuum (UHV) low temperature STM-MBE joint system (Unisoku

dilution LT UHV STM with SC Magnet USM1600). The $2H\text{-NbSe}_2$ substrate was synthesized by chemical vapor transport (CVD) method and *in situ* cleaved in UHV with base pressure 1×10^{-10} Torr. Bi_2Te_3 film was then grown on the substrate at 500 K using standard Knudsen cell sources. STM/STS measurements were taken at a nominal temperature of 30 mK with $^3\text{He}/^4\text{He}$ dilution refrigerator. Electrochemically etched W tips were adopted for normal topography and spectroscopy measurements, and Fe-coated W tips spin polarization measurements. dI/dV spectra were taken via the lock-in technique with a modulation of 0.1 mV at frequency of 991 Hz, and a set point of 0.2 nA. dI/dV mapping of vortices was measured at zero bias with a set point of 0.1 nA and feedback loop off. All STS curves were normalized to the dI/dV value of the spectra at bias energy outside the superconducting gap, so that the intensities of the ZBP under the four field-tip configurations can be compared to each other.

The Abrikosov vortex has recently been observed on a TI/SC heterostructure [14]. At the center of the vortex core, a typical ZBP can be seen. Because of the existence of MZM on TI/SC, the splitting of the spectra of the core states from the center shows a Y shape, deviating from the V shape in the usual SC [15,18,19]. Figure 2(a) shows the mapping of one 5QL $\text{Bi}_2\text{Te}_3/\text{NbSe}_2$ sample. The out-of-plane magnetic field applied on sample was $B = 0.1$ T. The size of the vortex was approximately 80 nm.

Fe coated W tips were adopted to study the ZBP at the vortex core of the TI/SC 5 QL sample. Prior to the deposition of Fe atoms, the W tip was annealed at a temperature over 2200 K to remove oxide layers. A magnetic field of 2.0 T perpendicular to the plane was applied on and then removed gradually from such a ferromagnetic tip, to obtain an up or down tip polarization. The applied external field to generate vortices on the sample is $B = 0.1$ T, which is smaller than the recovery field of the tip [20]. Thus, a ferromagnetic tip with out-of-plane polarization (\uparrow or \downarrow) can be used to detect the spin property of the ZBP. In Fig. 2(b), we show the normalized ZBP spectra probed at the vortex center by using an Fe/W tip of $M\uparrow$ and $M\downarrow$ at $B = 0.1$ T(\uparrow). Clearly, the ZBP in the parallel field-tip configuration (red) is higher than the ZBP in the antiparallel configuration. To eliminate the possible effect of spatial anisotropy to the spin-dependent tunneling conductance, we carried out the same measurements by reversing B from 0.1 T(\uparrow) to 0.1 T(\downarrow). As shown in the two right subpanels in Fig. 2(b), the height of the ZBP is found higher again in the parallel configuration. Since the normal tunneling contribution to the ZBP is essentially independent of the spin [see model calculation part, Fig. 3(b)], the spin dependent ZBP is in full agreement with the novel property of the MZM to induce spin selective AR. We have measured the conductance far from the center of the vortex, and found that the conductance is essentially independent of the spin polarization. Figure 2(c)

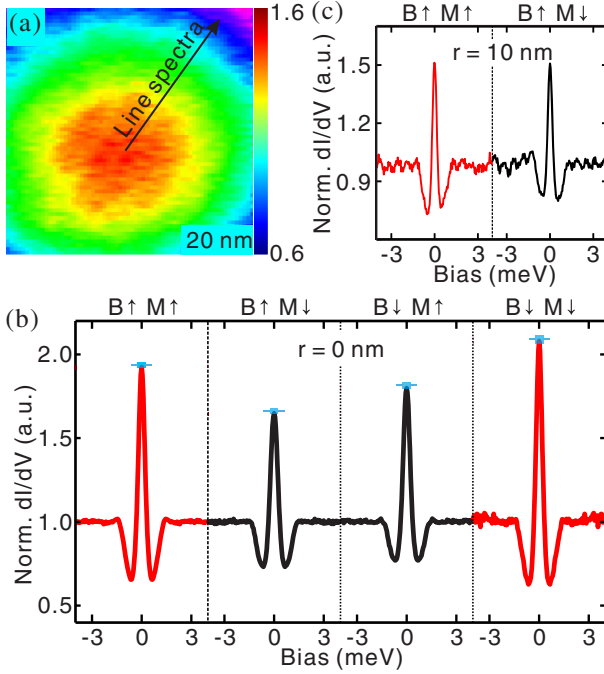


FIG. 2. (a) Zero bias dI/dV mapping of a vortex at 0.1 T with the spin nonpolarized tip on the topological superconductor 5QL $\text{Bi}_2\text{Te}_3/\text{NbSe}_2$. (b) dI/dV at the vortex center measured with a fully spin polarized tip. Red curves are for tip polarization M parallel to magnetic field B , and black curves are for M antiparallel to B . In the measurements, $B = 0.1$ T and temperature $T = 30$ mK. The blue lateral lines give the average values of the intensities in multimeasurements, the vertical bars are the standard error bars. The intensity of the conductance with M parallel to B is about 14% higher than that with M antiparallel to B . (c) dI/dV at 10 nm away from the center of a vortex measured with a fully spin polarized tip, where the tunneling is found independent of the spin polarization.

shows dI/dV at $r = 10$ nm, which is independent of the spin. Therefore, the spin dependence of the tunneling is a property at the vortex center, in further support of the scenario of the SSAR of the MZM.

To make the analyses more quantitative, we define spin polarization of the tunneling conductance at zero bias,

$$P(B\uparrow) = \frac{G(B\uparrow, M\uparrow) - G(B\uparrow, M\downarrow)}{G(B\uparrow, M\uparrow) + G(B\uparrow, M\downarrow)}, \quad (2a)$$

and

$$P(B\downarrow) = \frac{G(B\downarrow, M\downarrow) - G(B\downarrow, M\uparrow)}{G(B\downarrow, M\downarrow) + G(B\downarrow, M\uparrow)}, \quad (2b)$$

where $G(B\uparrow, M\uparrow) = dI(B\uparrow, M\uparrow)/dV$ is a spin polarization dependent conductance at zero bias. The values of $P(B\uparrow)$ and $P(B\downarrow)$ obtained for $r = 0$ from the data in Fig. 2(b) are about 7%, which corresponds to a relative increase of about 14% for the parallel configurations. $P(B)$

for $r = 10$ nm is essentially zero. As we will discuss below, $P(B)$ is observed to vanish in conventional SC.

To model the 5QL $\text{Bi}_2\text{Te}_3/\text{NbSe}_2$ heterostructure, we consider the surface of a 3D TI described by a Rashba spin-orbit coupled system [21,22], $H_0 = \alpha(\vec{s} \times \vec{p}) \cdot \hat{z}$ with \hat{z} the normal direction to the surface, and its superconductivity is induced through the proximity to an s -wave SC. We assume a single vortex is created by an external magnetic field, while the Zeeman splitting effect is much smaller than the orbital effect and can be neglected. By solving Bogoliubov-de Gennes equations, we find a MZM inside the vortex core along with low lying quasiparticle states within the superconducting gap. The energy separation of these low lying quasiparticle states may be estimated as Δ/E_f , with Δ the bulk SC gap and E_f the Fermi energy, which is much smaller than the energy resolution 0.1 meV of the STM for the present sample. Typically there are over a dozen low lying quasiparticle states within 0.1 meV. The differential tunneling conductance measured by STM at the spatial point of the vortex core center $r = 0$, however, is much simpler. At $r = 0$, only the MZM and the first low lying excited quasiparticle state have nonzero wave function amplitudes. All the other quasiparticle states have a zero amplitude; hence, they can be neglected for the present study of STM at $r = 0$. The wave functions of the MZM and the first low lying excited quasiparticle state are illustrated in Fig. 3(a). The spin distribution of these low lying states are determined by the Rashba coupling together with superconducting order parameter. The spin polarization at $r = 0$ is found to be up (along the magnetic field) for the MZM and down for the first low lying quasiparticle state, which may be attributed to the fact that the Rashba coupling is caused by broken mirror symmetry at the surface and the rotation around the normal direction to the surface is still invariant.

The Fe coated STM tip is modeled by a SP metallic lead, which couples to the TI surface through a point contact at $r = 0$. The junction setup is very similar to that used by He *et al.* [16], except that we use a 2D Rashba system instead of 1D quantum wire. We found that the AR contribution to the conductance, $dI(B\uparrow, M\uparrow)/dV|_A = 2e^2/h$, as plotted in Fig. 3(b), while $dI(B\uparrow, M\downarrow)/dV|_A$ vanishes, which are the same as those obtained in the 1D wire [16]. Note that the superconducting order parameter is zero at the vortex center $r = 0$, so that the only AR is via the MZM. The total tunneling conductance has a normal tunneling part, or the first term in Eq. (1). The relative weight between the two terms depends on the tunneling barrier. To make a comparison with experiment, we consider the limit of the transparent barrier to estimate $dI(r, E)/dV|_n \sim 0.88e^2/h$ for a given spin in the normal state, and obtain $dI(r = 0, E = 0)/dV|_n = dI(r, E)/dV|_n N(r = 0, E = 0)/N(r, E)$ with $N(r, E)$ the local density of states for the given spin [23]. The results for the total tunneling conductance [24,25] in Eq. (1) are plotted in Fig. 3(c). We estimate $P[B\uparrow(\downarrow)] = 17\%$, which

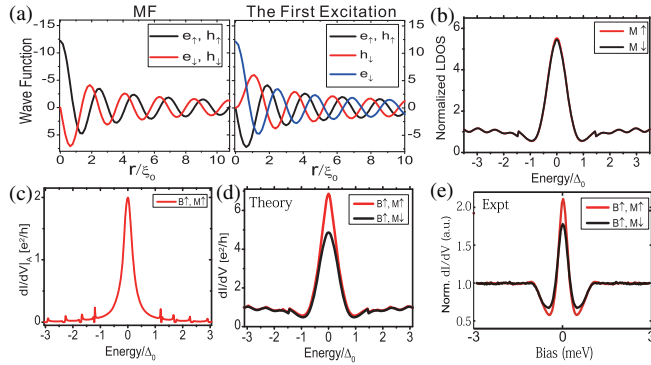


FIG. 3. Model calculations for spin selective AR at the center of the vortex core in the 2D topological superconductor. (a) The wave function of the MZM (left) and the first low lying quasiparticle state (right) inside a vortex core with magnetic field B upward. Spin components (\uparrow, \downarrow) of electron [e] and hole [h] are indicated in the figure. Note that the local spin at $r = 0$ for MZM is completely up. (b)–(e) Properties at vortex center $r = 0$. (b) Normalized local density of states for spin \uparrow and spin \downarrow (black), which are essentially the same within the energy resolution. (c) Calculated AR conductance for the tip spin polarization M parallel to B . The AR conductance is zero for M antiparallel to B . (d) Spin-dependent tunneling conductance in Eq. (1) estimated in a transparent limit. The red (black) curve is for M parallel (antiparallel) to B . (e) The same as in (d), for experimentally measured conductance. In the calculations [26] we set the superconducting gap $\Delta_0 = 1$ (1 meV in experiment) as the energy unit, the size of the vortex ξ_0 (35 nm in experiment) as the length unit defined as the distance from the center at which the superconducting gap $\Delta(\xi_0) = \tanh(1)\Delta_0$, and $\alpha = 35$ nm, and Fermi energy $E_f = 100$. The obtained first excited state energy is 0.04. We use energy broadening width $\eta = 0.4$, and the hopping between the lead and the vortex core center $\alpha = 35$. Note that the MZM and the first low lying excited state are primary states to contribute to the tunneling conductance at $r = 0$ (see the text).

is 2.4 times the experimental value of 7%. Figure 3(e) is a plot of measured spin-dependent dI/dV in the STM/STS, which compares with Fig. 3(d) of the theory quite well.

To further investigate the origin of the spin polarization dependence of the conductance, we have carried out a series of SP-STS measurements of the vortex core state on conventional superconductors, 3QL Bi_2Te_3 on top of NbSe_2 and bare NbSe_2 samples for comparison, where we do not expect the MZM [15]. The results are shown in Figs. 4(a) and 4(b), in which four panels represent four external field-tip polarization configurations. As we can see clearly, the STS in 3QL Bi_2Te_3 and NbSe_2 show little difference in the ZBP strength between the parallel and antiparallel field-tip configuration for either positive field $+0.1$ T or the negative one. The values of $|P(B\uparrow(\downarrow))|$ for 3QL Bi_2Te_3 and NbSe_2 samples are smaller than 1%. This is contrary to the spin-dependent ZBP observed in 5QL $\text{Bi}_2\text{Te}_3/\text{NbSe}_2$.

As the external magnetic field increases, the distance between the vortex decreases, and the interaction between vortices becomes stronger, which may destroy the MZM.

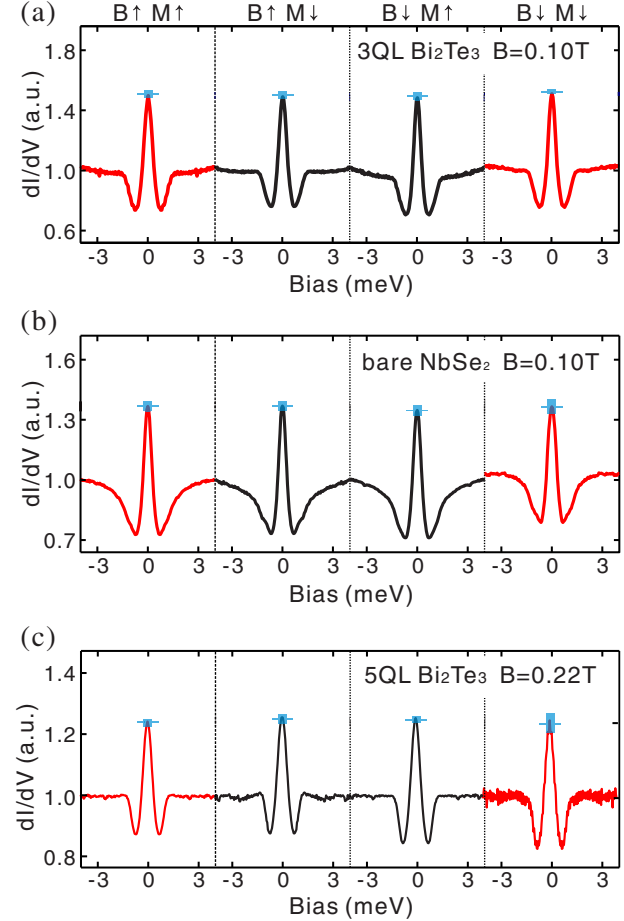


FIG. 4. dI/dV curves at the center of a vortex core measured with a fully spin polarized tip. Red curves are for polarization M parallel to B , and black curves are for M antiparallel to B . (a) and (b) for 3QL Bi_2Te_3 on NbSe_2 and bare NbSe_2 . In the measurements, $B = 0.1$ T. (c) for 5QL Bi_2Te_3 on NbSe_2 at $B = 0.22$ T. The measurement temperature $T = 30$ mK for all curves. The blue lateral lines give the average values of the intensities in multimeasurements; the vertical bars are the standard error bars.

inside vortices [15]. The SP STS measurements were also done at large magnetic fields for the 5QL $\text{Bi}_2\text{Te}_3/\text{NbSe}_2$ sample and the results are shown in Fig. 4(c). From which, we can see that the spin-selective tunneling effects disappear when the magnetic field is larger than 0.22 T. This also rules out the possibility that the SSAR is induced between the spin-polarized tip and the superconductor (with a strong spin-orbit coupling at surface). All these results demonstrate that the MZMs exist inside the vortices of the 5QL $\text{Bi}_2\text{Te}_3/\text{NbSe}_2$ sample at a field lower than 0.22 T, and spin-selective tunneling effects can be used to detect MZMs.

The spin selective AR was observed at the center of the vortex core on 5QL Bi_2Te_3 films grown on NbSe_2 at 0.1 T. In this nonmagnetic system, only the MZM can induce the spin selective AR. Together with the nonselective signal obtained in other comparison systems, our work gives definitive evidence of the MZM. It also suggests that spin

selective AR can be used in detection of the MZM in 3D TI/SC heterostructures and other systems that host MZMs with related spin-resolved techniques, MZMs can be manipulated by the interaction between vortices. In addition, the spin current from the MZM can be potentially used for spintronics.

We thank Chui-Zhen Chen, Wei-Qiang Chen, Jun He, K. T. Law, Qiang-Hua Wang, and Dong-Hui Xu for stimulating discussions. We wish to thank the Ministry of Science and Technology of China (Grants No. 2013CB921902, No. 2014CB921201, No. 2014CB921203, No. 2014CB921103, No. 2013CB922103, No. 20130073120081, No. 2012CB927401), NSFC (Grants No. 11521404, No. 11227404, No. 11274269, No. 11374256, No. 11374140, No. 11504230 No. 11574202 No. 11134008, No. 11374206, No. 11274228, No. 11574201) for partial support. H-H. S. and K-W. Z. conducted the experiments with the help of G. Y. W. and H. Y. M. S. C. L. provides all the support for the experiments and supervised K-W. Z. L. H. H. and C. L. carried out the calculations with the help from Y. Z., L. F., and F. C. Z. J. F. J. designed the experiments with the help from F. C. Z. Z. A. X. provided NbSe₂ crystals. S. C. L., C. L. G., D. D. G., C. H. L., D. Q., L. F., F. C. Z., and J. F. J. analyzed the data. H-H. S., F. C. Z., and J. F. J. wrote most of the Letter. All the authors discussed the results.

H-H. S. and K-W. Z. contributed equally to this work.

^{*}Corresponding author.

scli@nju.edu.cn

[†]Corresponding author.

fuchun@zju.edu.cn

[‡]Corresponding author.

jfjia@sjtu.edu.cn

- [1] E. Majorana, Teoria simmetrica dell'elettrone e del positrone, *Nuovo Cimento* **14**, 171 (1937).
- [2] F. Wilczek, Majorana returns, *Nat. Phys.* **5**, 614 (2009).
- [3] S. R. Elliott and M. Franz, Colloquium: Majorana fermions in nuclear, particle, and solid-state physics, *Rev. Mod. Phys.* **87**, 137 (2015).
- [4] C. Nayak, S. H. Simon, A. Stern, M. Freedman, and S. Das Sarma, Non-Abelian anyons and topological quantum computation, *Rev. Mod. Phys.* **80**, 1083 (2008).
- [5] S. Das Sarma, C. Nayak, and S. Tewari, Proposal to stabilize and detect half-quantum vortices in strontium ruthenate thin films: Non-Abelian braiding statistics of vortices in a $p_x + ip_y$ superconductor, *Phys. Rev. B* **73**, 220502 (2006).
- [6] G. Moore and N. Read, Nonabelions in the fractional quantum hall effect, *Nucl. Phys.* **B360**, 362 (1991).
- [7] L. Fu and C. L. Kane, Superconducting Proximity Effect and Majorana Fermions at the Surface of a Topological Insulator, *Phys. Rev. Lett.* **100**, 096407 (2008).
- [8] V. Mourik, K. Zuo, S. M. Frolov, S. R. Plissard, E. P. A. M. Bakkers, and L. P. Kouwenhoven, Signatures of Majorana fermions in hybrid superconductor-semiconductor nanowire devices, *Science* **336**, 1003 (2012).

- [9] M. T. Deng, C. L. Yu, G. Y. Huang, M. Larsson, P. Caroff, and H. Q. Xu, Anomalous Zero-Bias Conductance Peak in a Nb-InSb Nanowire-Nb Hybrid Device, *Nano Lett.* **12**, 6414 (2012).
- [10] A. D. K. Finck, D. J. Van Harlingen, P. K. Mohseni, K. Jung, and X. Li, Anomalous Modulation of a Zero-Bias Peak in a Hybrid Nanowire-Superconductor Device, *Phys. Rev. Lett.* **110**, 126406 (2013).
- [11] E. J. H. Lee, X. Jiang, M. Houzet, R. Aguado, C. M. Lieber, and S. De Franceschi, Spin-resolved Andreev levels and parity crossings in hybrid superconductor–semiconductor nanostructures, *Nat. Nanotechnol.* **9**, 79 (2014).
- [12] S. Nadj-Perge, I. K. Drozdov, J. Li, H. Chen, S. Jeon, J. Seo, A. H. MacDonald, B. A. Bernevig, and A. Yazdani, Observation of Majorana fermions in ferromagnetic atomic chains on a superconductor, *Science* **346**, 602 (2014).
- [13] M.-X. Wang *et al.*, The coexistence of superconductivity and topological order in the Bi₂Se₃ thin films, *Science* **336**, 52 (2012).
- [14] J.-P. Xu *et al.*, Artificial Topological Superconductor by the Proximity Effect, *Phys. Rev. Lett.* **112**, 217001 (2014).
- [15] J.-P. Xu *et al.*, Experimental Detection of a Majorana Mode in the core of a Magnetic Vortex inside a Topological Insulator-Superconductor Bi₂Te₃/NbSe₂ Heterostructure, *Phys. Rev. Lett.* **114**, 017001 (2015).
- [16] J. J. He, T. K. Ng, P. A. Lee, and K. T. Law, Selective Equal-Spin Andreev Reflections Induced by Majorana Fermions, *Phys. Rev. Lett.* **112**, 037001 (2014).
- [17] A. Haim, E. Berg, F. von Oppen, and Y. Oreg, Signatures of Majorana Zero Modes in Spin-Resolved Current Correlations, *Phys. Rev. Lett.* **114**, 166406 (2015).
- [18] T. Kawakami and X. Hu, Evolution of Density of States and a Spin-Resolved Checkerboard-Type Pattern Associated with the Majorana Bound State, *Phys. Rev. Lett.* **115**, 177001 (2015).
- [19] Z.-Z. Li, F.-C. Zhang, and Q.-H. Wang, Majorana modes in a topological insulator/s-wave superconductor heterostructure, *Sci. Rep.* **4**, 6363 (2014).
- [20] R. Wiesendanger, Spin mapping at the nanoscale and atomic scale, *Rev. Mod. Phys.* **81**, 1495 (2009).
- [21] J. D. Sau, S. Tewari, R. M. Lutchyn, T. D. Stanescu, and S. Das Sarma, Non-Abelian quantum order in spin-orbit-coupled semiconductors: Search for topological Majorana particles in solid-state systems, *Phys. Rev. B* **82**, 214509 (2010).
- [22] J. D. Sau, R. M. Lutchyn, S. Tewari, and S. Das Sarma, Robustness of Majorana fermions in proximity-induced superconductors, *Phys. Rev. B* **82**, 094522 (2010).
- [23] F. Gygi and M. Schlüter, Self-consistent electronic structure of a vortex line in a type-II superconductor, *Phys. Rev. B* **43**, 7609 (1991).
- [24] K.-Y. Yang, K. Huang, W.-Q. Chen, T. M. Rice, and F.-C. Zhang, Andreev and Single-Particle Tunneling Spectra of Underdoped Cuprate Superconductors, *Phys. Rev. Lett.* **105**, 167004 (2010).
- [25] D. Wang and Q. H. Wang, Model for Determining the Pairing Symmetry and Relative Sign of the Energy Gap of Iron-Arsenide Superconductors using Tunneling Spectroscopy, *Phys. Rev. Lett.* **102**, 197004 (2009).
- [26] L. H. Hu *et al.* (to be published).